IEEE Access
Multidisciplinary ⋮ Rapid Review ⋮ Open Access Journal

Received March 5, 2021, accepted March 23, 2021, date of publication April 1, 2021, date of current version April 13, 2021.

Digital Object Identifier 10.1109/ACCESS.2021.3070492

A Time Modulated Array With Polarization Diversity Capability

MOHAMMAD HOSSEIN MAZAHERI[1], (Member, IEEE), MOHAMMAD FAKHARZADEH[1], (Senior Member, IEEE), MAHMOOD AKBARI[1], AND SAFIEDDIN SAFAVI-NAEINI[2], (Life Fellow, IEEE)

[1]Department of Electrical Engineering, Sharif University of Technology, Tehran 11365-11155, Iran
[2]Centre for Intelligent Antenna and Radio Systems, University of Waterloo, Waterloo, ON N2L 3G1, Canada

Corresponding author: Mohammad Fakharzadeh (fakharzadeh@sharif.ir)

This work was supported in part by the National Science and Engineering Research Council (NSERC) of Canada, and in part by C-COM Satellite Systems.

ABSTRACT The Time Modulated Array (TMA) provides multiple radiation beams at different frequencies, by turning the radiating elements on and off. In this paper, we propose to add polarization diversity to a wireless communication link by leveraging the capabilities of the TMA. The proposed architecture switches between two orthogonal polarizations, instead of turning the antenna off, providing polarization diversity for the receivers. We show that the beams of each polarization at the sidebands are exactly the same. However, the switching sequence should be optimized for the fundamental frequency to provide the same radiation level at each sideband. Two different switching sequences are proposed, which are optimized for different conditions. To evaluate the switching sequences and the diversity order of the system, an 8-element array with dual polarization antennas is fabricated. The radiating antenna element is a dual feed ring slot antenna, designed for 5.8 GHz with 10% fractional bandwidth. Both the single antenna and the array are measured in an anechoic chamber. The measurements indicate that the prototype provides full diversity gain along with multiple beam generation and beam steering, while it is very low cost and has low complexity.

INDEX TERMS Antenna array, time modulated array, polarization diversity, efficiency, wireless communication.

I. INTRODUCTION

The Time-Modulated Array (TMA) has been introduced as a promising architecture for array beamforming. The main benefits of the TMA are twofold; first, the TMA has comparably a lower cost than a phased array system since it only uses (Radio Frequency) RF Single Pole Double Throw (SPDT) switches rather than expensive phase shifters [1]. The other benefit is the ability of the TMA to produce multiple simultaneous radiation beams at different angles [2]. Both these benefits have made TMA suitable for low-cost and versatile beamforming architecture.

The TMA periodically switches each antenna element on and off. The switching frequency (f_p) is much lower than the carrier frequency (f_0) [3]. As a result, the output of the system has harmonics or sidebands at $f_0 \pm mf_p$, where m is the number of the sideband. Since the switching sequence of each antenna is different from the others in the array, the radiation beam of the array at the sidebands can be shaped and steered toward the desired angles. Different beamsteering and beamshaping techniques are proposed and implemented for various applications [4]–[8].

The capabilities of TMA have made it suitable to fulfill the requirements of the modern wireless communication link, by properly aligning the radiation beam at each sideband. The performance of the TMA is compared with a phased array, in terms of noise figure in the receiver [9] and active impedance in the transmitter side [10]. Both indicate the potential of a TMA to meet the requirements of wireless technologies. In [11], a TMA architecture is proposed as a multi-user Access Point (AP). The TMA architectures for both up-link and down-link are proposed using only one RF chain, which reduces the cost and power consumption of the receiver. In addition, in [12] the capability of TMA to reject unwanted interference in a Global Positioning System (GPS) receiver is demonstrated. The considerations of sending

The associate editor coordinating the review of this manuscript and approving it for publication was Davide Ramaccia.

data through a TMA structure is investigated in [3] and recently,

Furthermore, TMA is proposed as a low-cost and simple architecture for beamforming for the emerging mm-wave communication systems [13], [14].

Although beamforming helps to direct the beam toward the receiver, the wireless communication link is still vulnerable to the propagation environment.

Exploiting diversity techniques helps to overcome the propagation issues. Generally, diversity is added to the system by sending the same data in different times, frequencies, polarizations or even different directions in space [15]. Recently, a TMA with dual circular polarization is proposed where it can provide orthogonal circular polarizations in different sidebands [16]. However, the proposed setup is not scalable, only 4 antenna elements, and it is only suitable for 0° direction. In a diversity system, multiple copies of data are sent over two or more orthogonal paths, each signal experiences different fadings. Thus, the receiver should combine each signal according to the channel state. Generally, three different combining techniques are widely used in diversity systems; selection combining, equal gain combining and Maximal Ratio Combing (MRC) [17]. The MRC provides the best SNR among other combining techniques [18].

In a conventional TMA structure, the feed network is either connected to the radiating antenna or it is matched to a 50 Ω load. As a result, if the TMA is used as a transmitter, a fraction of power is dissipated in the matched load. In this paper, we propose a new architecture to implement a wireless communication link based on the polarization diversity. We employ the Complementary Mode Switching (CMS), which was introduced in [19] and [20] to switch between the two polarizations of the antenna, rather than turning the element off to increase the radiation efficiency. Consequently, the radiation pattern and the gain of each polarization are exactly the same at the sidebands.

In this paper, first the beamforming with TMA along with CMS principles are introduced in Section II. Then the system model is investigated, considering TMA as the transmitter. The diversity gain is introduced in Section III, which is used as a measure of system design and evaluation. In Section IV, two switching sequences are designed for two different scenarios with polarization diversity. In addition, the two beamforming scenarios are tested on a TMA prototype. The hardware details and measurement results that are provided in Section V of the paper show that the proposed architecture can steer the beam for different users at different angles and provide full polarization diversity for all of them at the same time.

II. TMA PRINCIPLES

A conceptual block diagram of the proposed dual polarized TMA is shown in Fig. 1, where the SPDT periodically switches between the two orthogonal polarizations. The period of all switches is the same but the switching sequences can be different. As a result, the weighting of each element

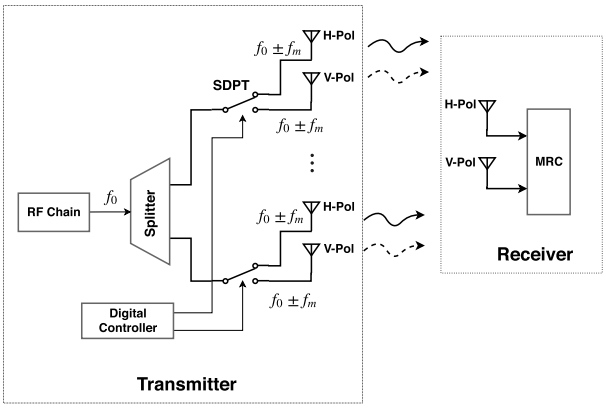

FIGURE 1. Proposed architecture for a TMA system with polarization diversity, where each SPDT switches between two polarizations.

varies with time and gain of the array at Horizontal polarization (H) is:

$$G_H(\theta) = \sum_{n=0}^{N-1} w_n(t) \cdot e^{jk_0 nd \cdot sin\theta};$$
$$w_n(t) = \begin{cases} 1 & 0 \le t_n^{on} < t < t_n^{off} \le T_p \\ 0 & otherwise \end{cases}, \quad (1)$$

where the $w_n(t)$ is the weight of the n^{th} element, k_0 is the wave-number at carrier frequency (f_0) and d is the distance between the antenna elements in the array. Since the $w_n(t)$ is a periodic function in time with period T_p ($= 1/f_p$), using Fourier series, the array weightings can be expanded in a series of exponential harmonics, which is henceforth called sidebands:

$$w_n(t) = \sum_{m=-\infty}^{\infty} a_{mn} \cdot e^{j2\pi f_p t} \quad (2)$$

where the Fourier coefficients (a_{mn}) are:

$$a_{mn} = \frac{1}{T_p} \int_0^{T_P} w_n(t) \cdot e^{jm2\pi f_p t} dt \quad (3)$$

As a result, the array factor of the TMA at m^{th} sideband is:

$$G_H(\theta)\Big|_m = \sum_{n=0}^{N-1} a_{mn} \cdot e^{jk_0 nd.sin\theta} \quad (4)$$

It is necessary to consider the hardware limitations of the TMA, when designing the switching sequences. In [19] it was shown that each antenna can be on or off in specific time slots. The reason is twofold; one is the discrete time control from the digital controller, which emanates from the clock frequency of the digital controller. The second reason is the rise/fall time of the SPDT switches. To have rectangular pulse shapes, the switching period must be much higher than the rise/fall time of the switch. As a result, we consider the hardware limitation and employ the discrete switching time

array factor [19]:

$$G_H(\theta)\Big|_m = \sum_{n=0}^{N-1} \frac{1}{m\pi} e^{jk_0 nd sin\theta} \cdot e^{j\frac{2m\pi}{Q}} \cdot sin(\frac{m\pi}{Q}) \cdot V_n \quad (5a)$$

$$V_n = \sum_{q=1}^{Q} S_{qn} \cdot e^{-j2\pi m \frac{q}{Q}} \quad (5b)$$

The S_{qn} in (5) is the switching parameter, which is 1 or 0, determining that the n^{th} antenna is on or off within the q^{th} time slot among the total Q time slots. Therefore, we design proper switching sequence by determining each time slot to be on or off for each antenna rather than defining the t_n^{on} and t_n^{off} of the array.

Recently, the authors introduced the CMS algorithm to optimize the radiation efficiency [21]. In CMS, an inverted switching sequence is applied to the switches, which significantly improves the radiation efficiency in TMA. The inverted switching sequence in CMS is as follows:

$$w_n^c(t) = 1 - w_n(t), \quad (6)$$

where the superscript c represents the complement sequence. In [21], it was shown that when the switching sequence is inverted, as in CMS, the magnitude of the coefficients at the sidebands is the same, while the magnitude at the fundamental frequency is subtracted by 1:

$$a_{mn}^c = \begin{cases} 1 - a_{mn} & m = 0 \\ -a_{mn} & m \neq 0 \end{cases}. \quad (7)$$

According to Fig. 1, the vertical polarization is the CMS of the horizontal polarization. As a result, the radiation patterns at the sidebands are exactly the same for the two polarizations. However, the CMS does not provide the same patterns at fundamental frequency. In Section IV, proper switching sequences are designed to achieve the same radiation patterns at the fundamental frequency for each polarizations.

Since in a traditional TMA structure the antennas are turned off for a specific time duration, the total efficiency of TMA as a transmitter is lower than a conventional antenna array. The reason is that when an antenna is turned off, the corresponding feed network is connected to a matched load to dissipate the RF signal. On the other hand, in the proposed architecture shown in Fig. 1, the RF signal is propagated into the space through another antenna with orthogonal polarization, instead of dissipating power in a matched load. The two orthogonal polarizations can be used to increase the channel capacity or to provide polarization diversity for the wireless communication link. In the following sections we investigate the requirements of polarization diversity and propose optimized switching sequences to achieve the highest possible diversity order.

III. SYSTEM OVERVIEW

According to Fig. 1, each output port of a SPDT switch is connected to an antenna with a specific polarization. We assume that the antennas are providing Horizontal polarization (H-pol) and Vertical polarization (V-pol). To investigate the improvement of the proposed architecture, the system model is studied below.

A. SYSTEM MODEL

Assume that the signal $s(t)$ with power P_s is sent through the wireless channel in L orthogonal diversity branches. The received signal of the l^{th} branch at the receiver is:

$$r_l(t) = \sqrt{P_s} \cdot \sqrt{G_l} \cdot s(t) \circledast h_l(t) + n(t), \quad (8)$$

where G_l is the transmitter gain and l is either H or V polarization. Moreover, h_l is the channel response for the l polarization and $n(t)$ is the Additive White Gaussian Noise (AWGN) added to the system.

The channel response is a random function, where its statistical properties depend on the radiation environment. As a result, the averaged Signal to Noise Ratio (SNR) of the received signal at the l^{th} polarization is:

$$\overline{\Gamma_l} = \mathbb{E}\left[G_l \cdot |h_l|^2 \cdot \frac{E_b}{N_0}\right]$$
$$\overline{\Gamma_l} = G_l \cdot \mathbb{E}\left[|h_l|^2\right] \cdot \frac{E_b}{N_0}, \quad (9)$$

where $\mathbb{E}$ is the expectation of the random variable and E_b/N_0 is the bit energy to the noise power ratio.

We assume that the Maximal Ratio Combining (MRC) technique is utilized in the receiver to combine the received signals of each branch. The MRC employs the channel information in receiver and combines the received signals with proper weighting, so that the signal of each branch is added constructively. As a result, the averaged output SNR of the MRC receiver is:

$$\overline{\Gamma_c} = \sum_{l=1}^{L} \overline{\Gamma_l} \quad (10)$$

B. DIVERSITY GAIN AND BER

Generally, any type of diversity reduces the errors, which are emanated from the propagation channel. The variation of Bit Error Rate (BER) vs. SNR is a well-known metric to evaluate the performance of a wireless communication channel. Here, we assume that the receiver employs MRC to combine the received signals from L orthogonal branches. By assuming that the SNR of the diversity branches are statically independent, the output BER of the MRC becomes [22]:

$$BER = \int_0^\infty \dots \int_0^\infty P_S(e|\gamma_1 \dots \gamma_L) \prod_{l=1}^{L} p(\gamma_l) d\gamma_1 \dots d\gamma_L, \quad (11)$$

According to [23], the BER of an L-branch diversity system with an M-QAM modulation is:

$$BER = \frac{4}{\pi}(1 - \frac{1}{\sqrt{M}})$$

$$\times\Big\{\int_0^{\frac{\pi}{2}}\prod_{l=1}^{L}(1+\frac{3\overline{\Gamma_l}}{2(M-1)\sin^2\rho})^{-1}d\rho$$
$$-(1-\frac{1}{\sqrt{M}})\int_0^{\frac{\pi}{4}}\prod_{l=1}^{L}(1+\frac{3\overline{\Gamma_l}}{2(M-1)\sin^2\rho})^{-1}d\rho\Big\}, \quad (12)$$

where $\overline{\Gamma_l}$ is the averaged SNR of each branch, introduced in (9). Since we have two orthogonal polarizations, the number of branches in (12) is 2, $L = 2$, and we assume a 16-QAM modulation, $M = 16$, for the simulations.

Generally, by adding diversity to a system, the BER of the system reduces. The Diversity Gain (DG), introduced in [24] expresses the improvement of the BER due to the added diversity branch. DG is directly proportional to the decay of the BER with the increase of SNR. As mentioned, we have assumed the MRC is employed in the receiver, so the signal of each branch is added to the others with proper weighting. As a result, the DG becomes [24]:

$$DG = \frac{\overline{\Gamma_c}}{\overline{\Gamma_{ref}}} = \frac{P_c}{P_{ref}}, \quad (13)$$

where $\overline{\Gamma_c}$ and $\overline{\Gamma_{ref}}$ are the mean and maximum SNR among all the branches, respectively. Similarly, P_c is the power of the combined signal and P_{ref} is the power level of the reference branch, which is usually the branch with the maximum power. By replacing (9) and (10) into (13) and assuming that the variance of all channels are the same (Ω), the DG becomes:

$$DG = \frac{\sum_{l=1}^{L} G_l \cdot \Omega \cdot E_b/N_0}{G_{max} \cdot \Omega \cdot E_b/N_0} = \frac{\sum_{l=1}^{L} G_l}{G_{max}} = \sum_{l=1}^{L} |g_l|^2, \quad (14)$$

where g_l is the gain of each branch normalized to the maximum gain.

Consequently, in our proposed polarization diversity, it is important to provide the same radiation gain at each polarization to achieve the highest DG. This requirement is automatically satisfied at the sidebands of the TMA, since based on (7), the amplitude of the sidebands in both polarizations are exactly the same. However, this is not the case for the fundamental frequency, since according to (7) the a_{mn} and a^c_{mn} are one-complemented at the fundamental frequency.

IV. DESIGNING THE SWITCHING SEQUENCE

In this section we design a proper switching sequence for efficient polarization diversity system. As discussed in Section III, one parameter to design the switching sequence is the Diversity Gain (DG). We can reach full diversity with CMS at the sideband, regardless of switching sequence. To achieve a proper DG at the fundamental frequency, a proper switching sequence must be designed. The beamforming gain at the fundamental frequency and at the sidebands must be high enough to meet the requirements of the link budget.

One solution is to design a switching sequence in which the total on-time of each antenna is equal to the total off-time. Therefore, we choose the $a_{0n} = 0.5$ and $a^c_{0n} = 0.5$. Although this approach guarantees equal beamforming gain at the fundamental frequency for primary and CMS sequences, it is not the best solution, since it adds a limiting constraint on the switching sequence, which reduces the degree of freedom to design proper beamforming gain at the sidebands. Therefore, we utilize the Genetic Algorithm (GA) with the cost function (CF) defined bellow:

$$CF = \sum_k W_k \cdot \beta_k(\overline{S}), \quad (15)$$

where β_k is the k^{th} objective function and W_k is the weight of the objective function in the cost function. Moreover, the vector $\overline{S}$ is a set of S_{qn}, defined in (5).

The main goal of the optimization algorithm is to achieve the full diversity gain. Since the CMS automatically provides the same array gain for each polarization, the full diversity is achieved at the sidebands. Therefore, it is only required to optimize DG at the fundamental frequency. Based on (14), the optimization for DG results in the following objective function:

$$\beta_0 = \frac{|G_H(\theta) - G_V(\theta)|}{G_H(\theta)}\Big|_{m=0,\theta=0}, \quad (16)$$

where H and V polarizations are the CMS of each other. The objective function defined in (16) assures that the switching sequence provides equal array gain at the fundamental frequency for both polarizations. Note that the beam at the fundamental frequency is not steerable, thus (16) optimizes the beam at the broadside direction. In addition to (16), in (17) another objective function is defined at the 1^{st} sideband to obtain the maximum array gain for an arbitrary angle (θ_1). Note that θ_1 can be any angle within the scan range of the array.

$$\beta_1 = 10 \cdot log_{10}\{G_H(\theta)\big|_{m=1,\theta=\theta_1}\} - L_1 \quad (17)$$

According to [19], the maximum array gain of a TMA at its 1^{st} sideband for $N = 8$ and $Q = 20$ time slots is 4 dBi, without any additional constraint on the other sidebands. Therefore, for the first scenario we aim to optimize the array gain at the 1^{st} sideband, thus we choose $L_1 = 4\ dBi$. Replacing the objective functions defined in (16) and (17) into (15) and utilizing the GA optimization for $\theta_1 = 30°$ with 200 generations and population size of 100 gives the optimized switching sequence shown in Fig. 2(a). Note that in this figure the blue color represents the time that the signal is connected to the H-pol. The radiation patterns of the optimized switching sequence are depicted in Fig. 2(b). Since the radiation patterns of both polarizations at the sidebands are the same, the radiation patterns of V polarization at the sidebands are not shown in Fig. 2(b).

As reported in Fig. 2(b), the array gains at the fundamental frequency for both polarizations are almost the same (approximately 6 dBi). Even the corresponding radiation patterns are very similar except slight difference at the sidelobes, which are negligible. The gain values of TMA at $m = 1$ and $m = -1$

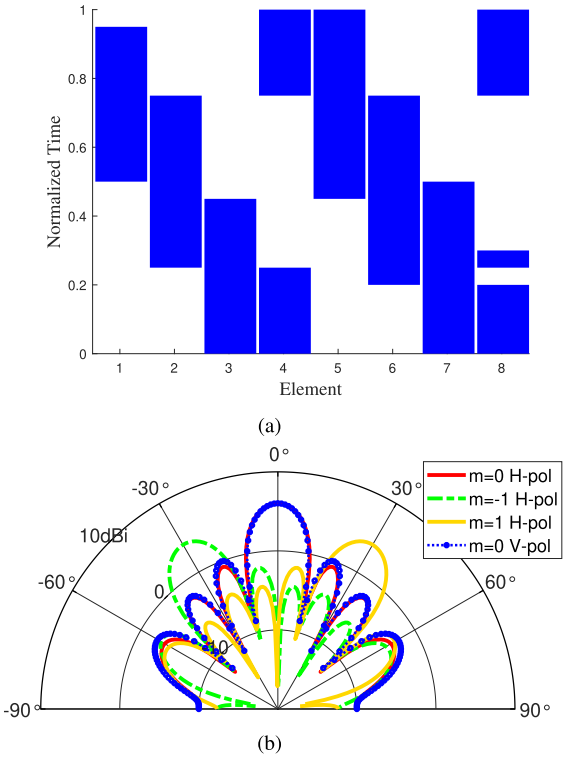

FIGURE 2. The optimization results of the first scenario (a) the switching sequence and (b) radiation patterns at each sideband.

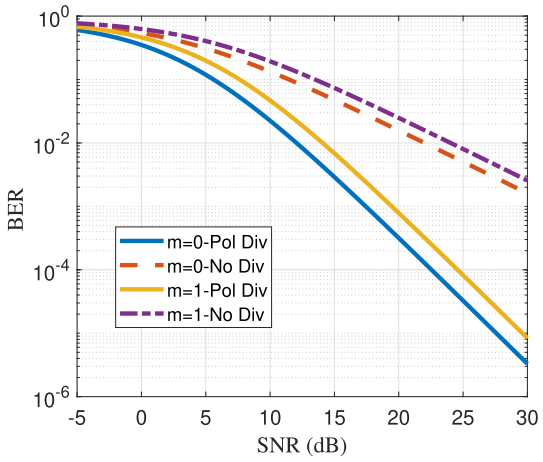

FIGURE 3. The BER versus SNR for a system with no diversity and a system with the optimized switching sequence for the first scenario.

TABLE 1. The radiation and diversity gain at each sideband for the second scenario.

Sideband number	Gain (dB)	DG
0	6	2
1	1.8	2
2	2	2

are about 3.99 dBi, which are very close to the desired levels. Note that according to (5b), the beam at the negative sideband has the same gain as its corresponding positive sideband but in the mirrored angle.

To evaluate the performance of the proposed structure, the BER variation versus SNR is shown in Fig. 3 for a system with and without polarization diversity. It indicates that the BER in a polarization diversity system is significantly reduced at the fundamental frequency and the 1^{st} sideband, compared to the no diversity system. According to [22], the slope of the BER curve at high SNR values represents the diversity gain, where Fig. 3 indicates that the slope of the polarization diversity curves are equal to 2. This verifies that the optimized switching sequence provides full diversity gain for the system. Note that the no diversity curve correspond to the traditional TMA, thus Fig. 3 indicates the advantage of the TMA with polarization diversity to the traditional one in terms of BER performance. The radiation patterns shown in Fig.2(b) are suitable to cover three users in 0 and $\pm 30°$ directions. The system is capable to cover other angles rather than $\pm 30°$ but to increase the number of covered users, another switching sequence must be designed.

In the second scenario, we design the beams to point at 0, $\pm 20°$ and $\pm 45°$ directions. Consequently, the cost function defined in (15) does not change. The other objective function is to maximize array gain at the 1^{st} and 2^{nd} sidebands simultaneously. Since no analytic bound is defined for this case, we define the objective function for the sidebands as follows:

$$\beta_1 = \frac{1}{G_H(\theta)}\Big|_{m=1,\theta=20°} \tag{18a}$$

$$\beta_2 = \frac{1}{G_H(\theta)}\Big|_{m=2,\theta=45°} \tag{18b}$$

The optimized switching sequence is shown in Fig. 4(a) and the corresponding radiation patterns at the positive sidebands are shown in Fig. 4(b). For the sake of simplicity, the radiation patterns of the negative sidebands are not shown in this figure. The direction of the beams are exactly the same as required, i.e. the beam corresponding to the fundamental frequency is toward the broadside direction, while the 1^{st} sideband is pointing at 20° and the beam of the 2^{nd} sideband is toward 45°.

The array gain and the DG of the optimized switching sequence, shown in Fig. 4(a) are summarized in Table 1. The optimized sequence provides almost the same array gain for both polarizations. Therefore, the DG reported in Table 1 is 2 for all sidebands and fundamental frequency. It is worth noting that in the second scenario, the array gain at the 1^{st} sideband is reduced compared to the first scenario. The reason is that the first constraint, β_0 in (16), implies a fixed radiation power at the fundamental frequency, hence, a part of the radiation power at the 1^{st} sideband is radiated at the 2^{nd} sideband. Although the TMA structure is capable to produce multiple beams to cover multiple directions simultaneously, the gain at each sideband drops by adding higher sidebands in the cost function. To overcome this limitation one can increase the number of antennas to provide more degrees of freedom in designing switching sequence.

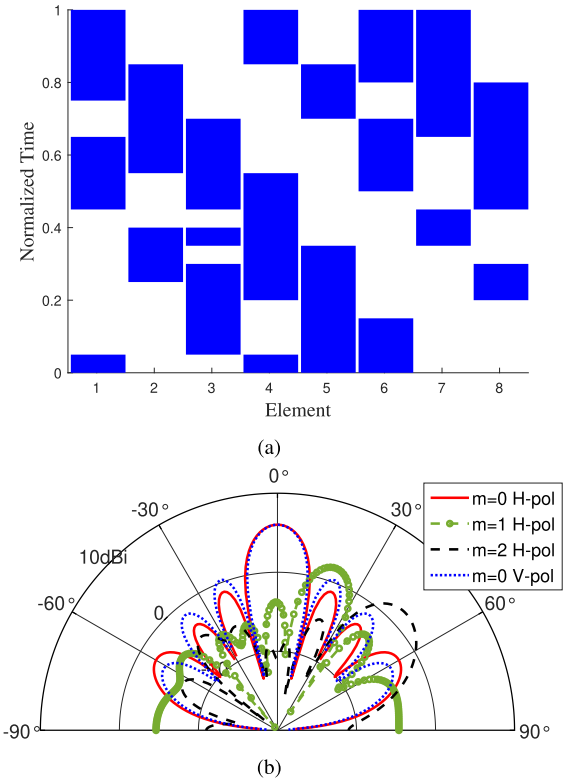

FIGURE 4. The optimization results of the second scenario (a) the switching sequence and (b) radiation patterns at each sideband.

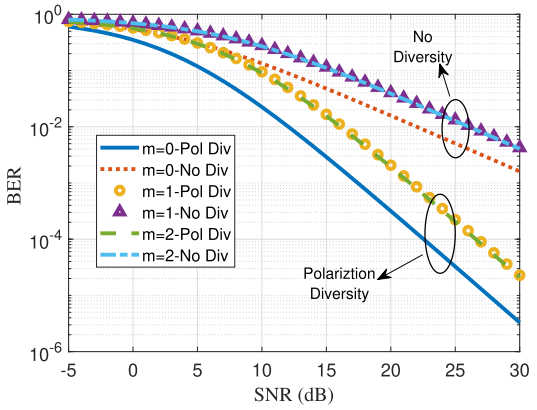

FIGURE 5. The BER versus SNR for a system with no diversity and a system with the optimized switching sequence for the second scenario.

The BER variation over SNR for the optimized switching sequence of Fig. 4(a) is depicted in Fig. 5 for the fundamental frequency and the two sidebands. The improvement of the polarization diversity system compared to the no-diversity system is investigated in Fig. 5. Similar to Fig. 3, the slope of the polarization diversity curves are about 2 at high SNR values, indicating that the optimized switching sequence reaches to the maximum diversity gain at each frequency band.

In terms of efficiency, the proposed architecture provides double times higher efficiency at sidebands compared to a conventional TMA. This is because the CMS provides exactly the same gain at the sideband, meaning that the wave is propagating with twice energy compared to conventional TMA. From energy point of view, the conventional TMA wastes part of the energy when the antenna is off, but the proposed architecture radiates that part of the energy into the space through an orthogonal polarization wave. This results in the efficiency improvement of the proposed architecture.

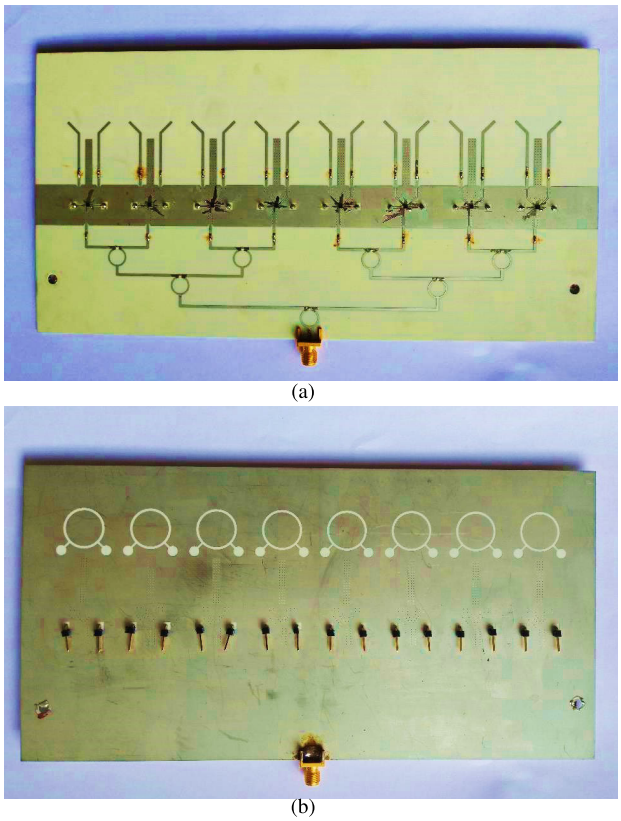

FIGURE 6. The fabricated 8-element TMA structure with SPDT switches and Wilkinson power distribution network (a) top view, (b) bottom view.

V. EXPERIMENTAL RESULTS

To evaluate the performance of the proposed polarization diversity system, a TMA beamforming architecture is developed along with dual polarized radiating elements. In this section we describe the details of the hardware implementation and evaluate the performance of the system.

A. HARDWARE IMPLEMENTATION

Fig. 6 illustrates the fabricated TMA structure, which is integrated with SPDT switches and radiating antenna elements. The beamforming network has a 1 to 8 Wilkinson power divider to equally deliver the input power to the 8 SPDTs. Each SPDT, switches between the two ports of its corresponding antenna to change the polarization of the radiated wave. The circuit is designed and fabricated on a Rogers 4003 substrate with 20 mil thickness and 3.66 for dielectric constant.

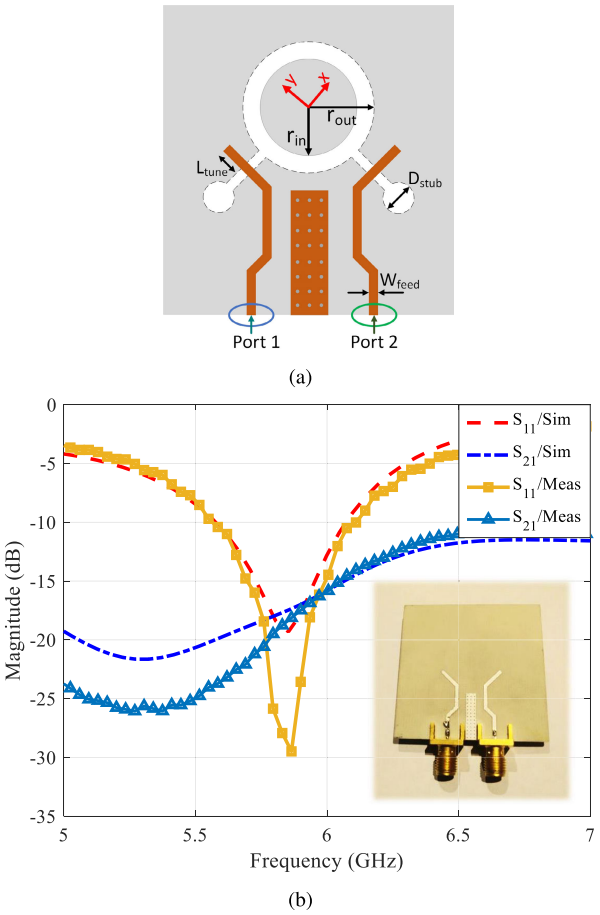

FIGURE 7. The single antenna structure (a) schematic view ($r_{in} = 7, r_{out} = 8, D_{stub} = 4, W_{feed} = 1.05, L_{tune} = 1$ all in mm) (b) Simulation and measurement results of S-parameter.

The radiating element of the array is a dual polarized planar antenna structure on the same substrate as the feed network, shown in Fig. 7. The dual polarized antenna is a compact two port ring slot antenna that supports two orthogonal linear polarizations. Moreover, it provides more than 10% bandwidth with using only a single layer substrate. As illustrated in Fig. 7(a), the ring slot is fed by a microstip line, passing the bottom of the board. A circular stub is utilized to match the impedance of the microstrip line to that of the ring slot. The scattering parameter of the fabricated prototype is shown in Fig. 7(b), where port 1 and port 2 are the feeding points of the antenna, providing orthogonal polarizations. Fig. 7(b) indicates that the antenna provides a good impedance matching at 5.8 GHz and the −10 dB impedance bandwidth ranges from 5.6 GHz to 6.2 GHz, which corresponds to more than 10% fractional bandwidth. In addition, the antenna has about 18 dB isolation between the two ports. There is a slight difference between the simulation and measurement result, which is mainly due to the metal losses that are not modeled in the simulation.

The radiation characteristics of the single antenna prototype are measured at 5.8 GHz. The measurements are done in the anechoic chamber in Centre for Intelligent Antenna

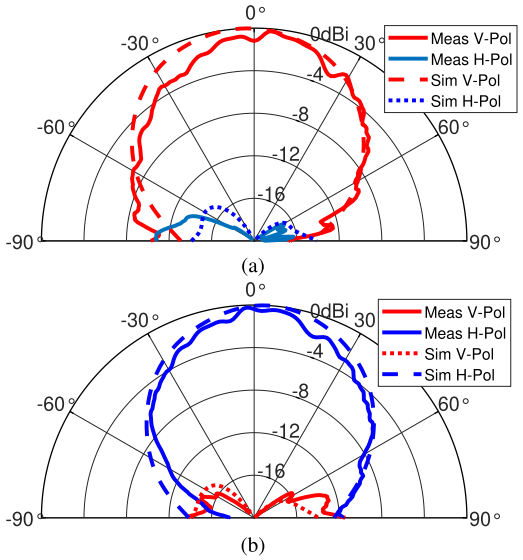

FIGURE 8. The simulated and measured radiation pattern of the dual-polarized antenna normalized to the maximum (a) port 1, (b) port 2.

and Radio Systems (CIARS) at the University of Waterloo. The normalized radiation patterns for port 1 and port 2 of the antenna are depicted in Fig. 8(a) and Fig. 8(b), respectively. These figures indicate that the measurement results of the single antenna prototype are in good agreement with the simulated ones. Moreover, the antenna gain is 4.8 dBi and the cross polarization of the proposed antenna is lower than −16 dB for angles between −45° to +45^o, suitable for the polarization diversity application.

The SKY13314-374LF switches are employed as the SPDT switch in the feed network of the TMA structure. As stated in the datasheet, the insertion loss of the SPDT is approximately −0.5 dB in the desired band and the switching time is 30 ns [25], which is fast enough for this design.

To characterize the SPDT performance, we have designed a test board, depicted in Fig. 9. The footprint of this switch urges the width of the transmission line to be narrow. Therefore, we designed proper Coplanar waveguide (CPW) lines to achieve the 50Ω impedance. Since the rest of the Printed Circuit Board (PCB) employs the microstrip transmission lines, a CPW to micristrip line transition is designed to connect the input and outputs of the SPDT to the rest of the feed network. To test the SPDT board, the common RF port and one of the output ports are connected to the network analyzer while the other output RF port of the SPDT is matched to a 50 Ω load. The insertion loss, scattering parameter and the isolation of the designed test board are illustrated in Fig. 9. According to the figure, the input and output of the SPDT are matched in the band of interest and the insertion loss is better than 1.6 dB. The reported insertion loss includes the loss of the SPDT (0.5 dB) along with the transmission lines, the CPW to microstrip transitions and the SMA connector. In addition, the isolation of the switch is better than 25 dB within the band of interest.

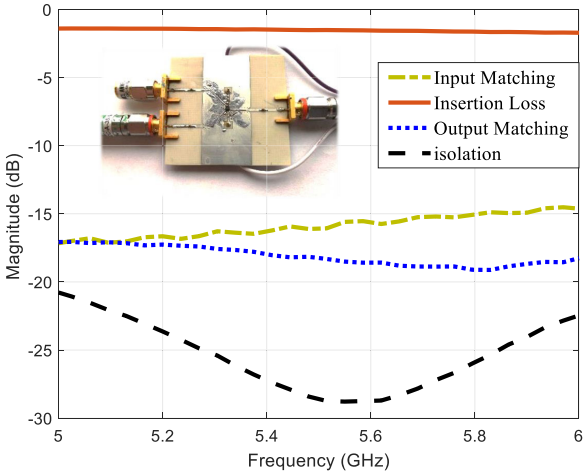

FIGURE 9. The fabricated test board for the SPDT and its performance.

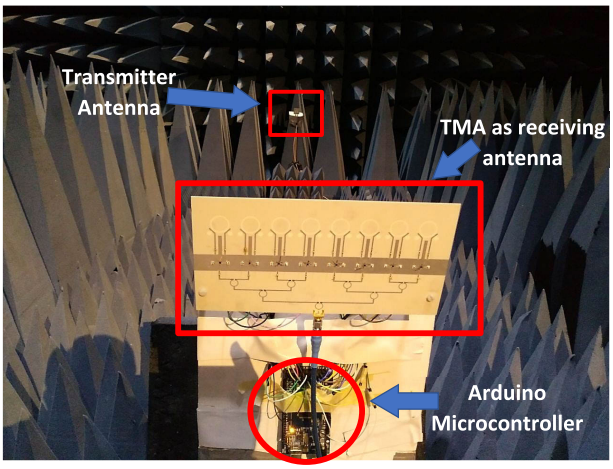

FIGURE 10. Antenna measurement setup, indicating the transmitter and AUT as the receiver.

B. TMA MEASUREMENT SETUP

The fabricated TMA structure, shown in Fig. 6, connects to a digital controller board to bias the switches and control the on and off time of each element. We have employed an Arduino Mega 2560 digital controller, with 16 MHz clock frequency [26]. The complete setup is tested in an anechoic chamber for measuring the radiation patterns corresponding to the proposed switching sequences.

The measurement setup is shown in Fig. 10, where a linear polarized antenna is connected to a signal generator, providing a continuous wave at 5.8 GHz. The TMA is connected to the spectrum analyzer and placed within 4 m from the transmitter to provide the far field condition. As depicted, the environment is completely covered by high performance absorbers to avoid reflections from different directions. Moreover, the modulation frequency (f_p) of the TMA is 100 kHz.

The measurement is executed for both linear polarizations (horizontal and vertical). The measured radiation patterns of the TMA for the proposed switching sequences are shown

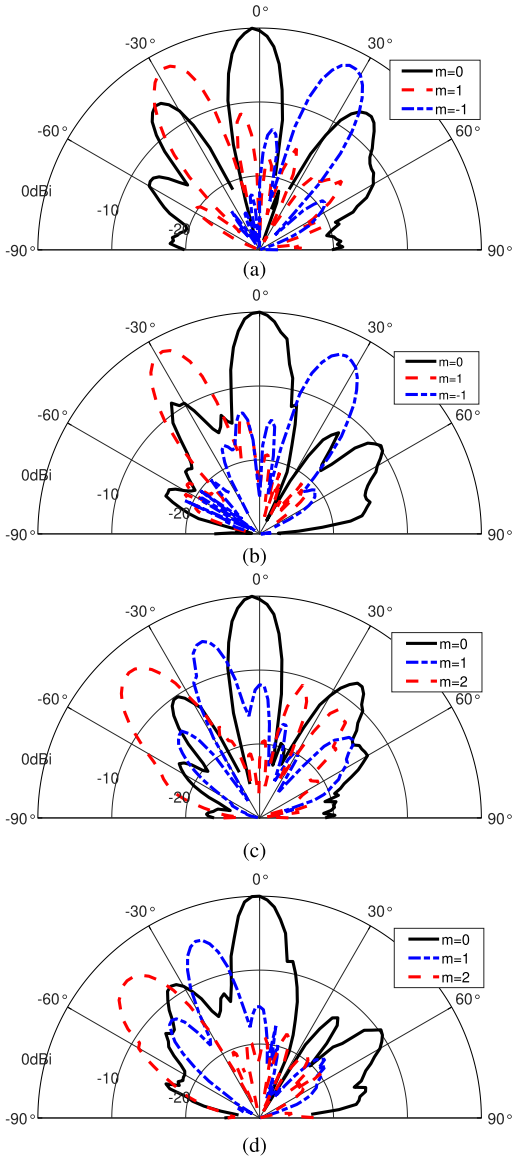

FIGURE 11. Measured radiation patterns of the fabricated TMA structure at the fundamental frequency and sidebands normalized to the maximum (a) first scenario H-polarization, (b) first scenario V-polarization, (c) second scenario H-polarization, (d) second scenario V-polarization.

in Fig. 11. Similar to the simulation results, the first positive and negative sidebands of the radiation patterns are shown in Fig. 11(a) and Fig. 11(b), while only two positive sidebands are shown in Fig. 11(c) and Fig. 11(d) to clearly illustrate the performance of the structure.

The radiation pattern at the 1^{st} sideband is approximately pointing toward $-30°$, similar to the simulation result, shown in Fig. 2(b). Moreover, the corresponding radiation patterns of the 2^{nd} scenario, shown in Fig. 11(c) and Fig. 11(d), indicate that the 1^{st} and 2^{nd} sidebands are respectively pointing toward $-20°$ and $-45°$, which is quite similar to Fig. 4(b).

Additionally, Table 2 indicates the gain at each sideband for the first scenario. The corresponding DG at each sideband can be easily calculated using (14). The DG is more than 1.93 for all of the sidebands, very close to the full diversity gain. Note

TABLE 2. The measured squared magnitude of the array factor at each sideband for the first scenario.

Sideband number	V-Pol (dB)	H-Pol (dB)
0	5.8	5.7
1	3.6	3.8
-1	3.7	3.4

TABLE 3. The measured squared magnitude of the array factor at each sideband for the second scenario.

Sideband number	V-Pol (dB)	H-Pol (dB)
0	5.4	5.7
1	1.6	1.4
-1	1.5	1.2
2	1.8	1.5
-2	1.9	1.5

that the antenna gain is subtracted from the measured values, so that in this table we only report the squared magnitude of the array factor so that it can be easily compared with the simulation values.

Similarly, Table. 3 indicates the measured gain of the array at each sideband for the switching sequence, designed for the second scenario. Similar to Table. 3, here the antenna gain is excluded from the reported values and the measured gains are close to the simulated ones. By using (14) and replacing measured gain for V and H polarization, the DG can be calculated for each sideband. The calculated DG of this switching sequence is above 1.9 for all of the sidebands, which again indicates that the proposed switching sequence and the fabricated setup represent the desired performance.

VI. CONCLUSION

In this paper we proposed a new architecture to leverage the capability of TMA in producing multiple radiation beams at different frequencies. The proposed architecture switches between the two different polarizations rather than turning the antenna on and off. As a result, the transmitter is always sending data to the receiver, therefore there is no radiation loss in TMA. Different switching sequences were presented, which aimed to optimize two or three radiation beams. The optimization constraints were designed to provide the highest diversity gain along with sufficient antenna gain at each sideband to meet the requirements of the wireless link budget.

To evaluate the performance of the proposed architecture and switching sequences, we implemented an 8-element TMA with half wavelength spacing. The antenna array was integrated with the feed network, which included RF SDPTs to switch between the antenna polarizations. The performance of the fabricated setup was measured in an anechoic chamber, which demonstrated similar radiation patterns as the simulation ones. Moreover, the measurements indicate that the diversity gain is always higher than 1.9, which is close to the theoretical value and provides a robust wireless communication link in a harsh environment.

ACKNOWLEDGMENT

The authors would like to thank the Centre for Intelligent Antenna and Radio Systems (CIARS) group for their help in fabrication and measurement process.

REFERENCES

[1] H. E. Shanks and R. W. Bickmore, "Four-dimensional electromagnetic radiators," *Can. J. Phys.*, vol. 37, no. 3, pp. 263–275, Mar. 1959.
[2] L. Poli, P. Rocca, G. Oliveri, and A. Massa, "Harmonic beamforming in time-modulated linear arrays," *IEEE Trans. Antennas Propag.*, vol. 59, no. 7, pp. 2538–2545, Jul. 2011.
[3] R. Maneiro-Catoira, J. C. Brégains, J. A. García-Naya, and L. Castedo, "On the feasibility of time-modulated arrays for digital linear modulations: A theoretical analysis," *IEEE Trans. Antennas Propag.*, vol. 62, no. 12, pp. 6114–6122, Dec. 2014.
[4] Y. Wang and A. Tennant, "MVDR beamforming applied to a time-modulated reflector-array," in *Proc. Loughborough Antennas Propag. Conf. (LAPC)*, Nov. 2013, pp. 591–594.
[5] L. Poli, P. Rocca, L. Manica, and A. Massa, "Handling sideband radiations in time-modulated arrays through particle swarm optimization," *IEEE Trans. Antennas Propag.*, vol. 58, no. 4, pp. 1408–1411, Apr. 2010.
[6] P. Rocca, Q. Zhu, E. T. Bekele, S. Yang, and A. Massa, "4-D arrays as enabling technology for cognitive radio systems," *IEEE Trans. Antennas Propag.*, vol. 62, no. 3, pp. 1102–1116, Mar. 2014.
[7] D. Masotti, "A novel time-based beamforming strategy for enhanced localization capability," *IEEE Antennas Wireless Propag. Lett.*, vol. 16, pp. 2428–2431, 2017.
[8] L. Poli, P. Rocca, and A. Massa, "Sideband radiation reduction exploiting pattern multiplication in directive time-modulated linear arrays," *IET Microw., Antennas Propag.*, vol. 6, no. 2, pp. 214–222, Jan. 2012.
[9] M. H. Mazaheri, M. Fakharzadeh, M. Akbari, and S. Safavi-Naeini, "A figure of merit in a time-modulated array," *IEEE Antennas Wireless Propag. Lett.*, vol. 18, no. 10, pp. 2086–2089, Oct. 2019.
[10] M. H. Mazaheri, M. Fakharzadeh, M. Akbari, and S. Safavi-Naeini, "Reduced active impedance variation by using time modulated array," in *Proc. IEEE Int. Symp. Antennas Propag. USNC-URSI Radio Sci. Meeting*, Jul. 2019, pp. 1765–1766.
[11] C. He, X. Liang, B. Zhou, J. Geng, and R. Jin, "Space-division multiple access based on time-modulated array," *IEEE Antennas Wireless Propag. Lett.*, vol. 14, pp. 610–613, 2015.
[12] M. H. Mazaheri, M. Fakharzadeh, M. Akbari, G. Shaker, and S. Safavi-Naeini, "Interference rejection with time modulated array for GPS application," in *Proc. IEEE Int. Symp. Antennas Propag. USNC/URSI Nat. Radio Sci. Meeting*, Jul. 2018, pp. 197–198.
[13] J. P. Gonzalez-Coma, R. Maneiro-Catoira, and L. Castedo, "Hybrid precoding with time-modulated arrays for mmWave MIMO systems," *IEEE Access*, vol. 6, pp. 59422–59437, 2018.
[14] J. P. Gonzalez-Coma and L. Castedo, "Power efficient scheduling and hybrid precoding for time modulated arrays," *IEEE Access*, vol. 8, pp. 21063–21076, 2020.
[15] D. Tse and P. Viswanath, *Fundamentals of Wireless Communication*. Cambridge, U.K.: Cambridge Univ. Press, 2005.
[16] G. Bogdan, P. Bajurko, and Y. Yashchyshyn, "Time-modulated antenna array with dual-circular polarization," *IEEE Antennas Wireless Propag. Lett.*, vol. 19, no. 11, pp. 1872–1875, Nov. 2020.
[17] D. Brennan, "Linear diversity combining techniques," *Proc. IRE*, vol. 47, no. 6, pp. 1075–1102, Jun. 1959.
[18] T. Eng, N. Kong, and L. B. Milstein, "Comparison of diversity combining techniques for Rayleigh-fading channels," *IEEE Trans. Commun.*, vol. 44, no. 9, pp. 1117–1129, Sep. 1996.
[19] M. H. Mazaheri, M. Fakharzadeh, and M. Akbari, "Efficiency enhancement of time-modulated arrays with optimized switching sequences," *IEEE Trans. Antennas Propag.*, vol. 66, no. 7, pp. 3411–3420, Jul. 2018.
[20] G. Bogdan, Y. Yashchyshyn, and M. Jarzynka, "Time-modulated antenna array with lossless switching network," *IEEE Antennas Wireless Propag. Lett.*, vol. 15, pp. 1827–1830, 2016.
[21] M. H. Mazheri, M. Fakharzadeh, and M. Akbari, "Efficiency improvement in TMA using complementary mode switching," in *Proc. IEEE Int. Symp. Antennas Propag. USNC/URSI Nat. Radio Sci. Meeting*, Jul. 2017, pp. 1601–1602.
[22] M. K. Simon and M.-S. Alouini, *Digital Communication Over Fading Channels*, vol. 95. Hoboken, NJ, USA: Wiley, 2005.

[23] R. Maneiro-Catoira, J. C. Bregains, J. A. Garcia-Naya, L. Castedo, P. Rocca, and L. Poli, "Performance analysis of time-modulated arrays for the angle diversity reception of digital linear modulated signals," *IEEE J. Sel. Topics Signal Process.*, vol. 11, no. 2, pp. 247–258, Mar. 2017.
[24] P.-S. Kildal, K. Rosengren, J. Byun, and J. Lee, "Definition of effective diversity gain and how to measure it in a reverberation chamber," *Microw. Opt. Technol. Lett.*, vol. 34, no. 1, pp. 56–59, Jul. 2002.
[25] *SKY13314-374LF: 0.1 to 6.0 GHz GaAs SPDT Switch*, SkyWorks Solutions Inc, Irvine, CA, USA, Jan. 2018.
[26] *Arduino Mega 2560*, Arduino, 2018.

MOHAMMAD HOSSEIN MAZAHERI (Member, IEEE) received the B.Sc. and M.Sc. degrees (Hons.) in electrical engineering from the Amirkabir University of Technology, Tehran, Iran, and the Ph.D. degree in electrical engineering from the Sharif University of Technology, Tehran, in 2019. Since 2019, he has been a Postdoctoral Fellow with the University of Waterloo, working on high-data-rate and low-power IoT devices and integrated phased array transceiver at mm-wave band. His main research interests include backscatter networks for high-data-rate and low-power communication systems, efficient beamforming techniques, the IoT networks, and mm-wave systems.

MOHAMMAD FAKHARZADEH (Senior Member, IEEE) received the M.Sc. degree in electrical engineering from the Sharif University of Technology, Tehran, Iran, in 2002, and the Ph.D. degree (Hons.) in electrical and computer engineering (ECE) from the University of Waterloo, Waterloo, ON, Canada, in 2008. He was the Manager of the Antenna and Packaging Group, Peraso Technologies, Toronto, ON, Canada, developing the integrated millimeter-wave solutions for portable electronic devices and small-cell backhaul. He is currently an Associate Professor with the Electrical Engineering Department, Sharif University of Technology, where he is also the Director of the Sharif University Incubator. He has over 20 years of experience in the design and implementation of the phased-array antenna and mm-wave systems, particularly novel antenna and packaging solutions. He has authored over 80 IEEE articles and holds ten U.S. patents.

MAHMOOD AKBARI received the B.S. degree from the University of Tehran, Tehran, Iran, in 1988, the M.S. degree from the Sharif University of Technology, Tehran, in 1993, and the Ph.D. degree from the Technical University of Hamburg-Harburg, Hamburg, Germany, in 2000, all in electrical engineering. He is currently an Associate Professor of electrical engineering with the Sharif University of Technology. He has experience in semiconductor laser devices, wave propagation in anisotropic media, and antenna theory. His current main research interests include wave propagation in periodic structures, meta materials, and photonic crystals.

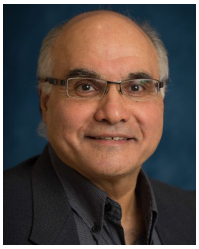

SAFIEDDIN (ALI) SAFAVI-NAEINI (Life Fellow, IEEE) received the B.Sc. degree in E.E. from the University of Tehran, Tehran, Iran, 1974, and the M.Sc. and Ph.D. degrees in E.E. from the University of Illinois at Urbana-Champaign, USA, in 1975 and 1979, respectively. He is currently a Professor with the Department of Electrical and Computer Engineering, University of Waterloo, and holds the NSERC/C-COM industrial research chair position with Intelligent Integrated Radio/Antenna Systems and Novel Electromagnetic Media Technologies. He is also the Director of the Center for Intelligent Antenna and Radio System (CIARS), University of Waterloo. He has published more than 200 journal articles and more than 400 conference papers in international conferences. His research interests include wide range of applications of electromagnetic devices and systems, including intelligent antennas and radio systems for emerging mobile networks and sensing (5G/6G, mobile satellite communication, and millimeter-wave radar), intelligent sensors for autonomous and hyper-connected car, millimeter-wave/THz integrated technologies with applications in imaging and bio-medical sensing, nano-EM and photonics, EM in bio-medical science, new EM materials, and computational methods. He has led several international collaborative research programs with research institutes in Germany, Finland, Japan, China, Sweden, and USA.